https://doi.org/10.5194/essd-2025-353
Preprint. Discussion started: 4 August 2025

Open Access Earth System Science Data Discussions

Spatiotemporal mapping of invasive yellow sweetclover blooms using Sentinel-2 and high-resolution drone imagery

Sakshi Saraf[1,*], Ranjeet John[1,2], Venkatesh Kolluru[2], Khushboo Jain[2], Geoffrey Henebry[3,4], Jiquan Chen[3,4], Raffaele Lafortezza[5]

*Corresponding author: Sakshi Saraf; Email: Sakshi.Saraf@coyotes.usd.edu; Orcid: 0000-0002-6785-8381

1. Department of Biology, University of South Dakota, Vermillion, SD 57069, USA
2. Department of Sustainability and Environment, University of South Dakota, Vermillion, SD 57069, USA
3. Department of Geography, Environment, and Spatial Sciences, Michigan State University, East Lansing, MI 48824, USA
4. Center for Global Change and Earth Observations, Michigan State University, East Lansing, MI 48823, USA
5. Department of Soil, Plant and Food Sciences (DISSPA), University of Bari "Aldo Moro", Via Amendola 165/A, 70126, Bari, Italy

https://doi.org/10.5194/essd-2025-353
Preprint. Discussion started: 4 August 2025

Open Access Earth System Science Data Discussions

Abstract

Yellow sweetclover (*Melilotus officinalis* (L.) Lam.; MEOF) is an invasive forb pervasive across the Northern Great Plains, often linked to traits such as wide adaptability, strong stress tolerance, and high productivity. Despite MEOF's prevalent ecological-economic impacts and importance, knowledge of its spatial distribution and temporal evolution is extremely limited. Here, we aim to develop a spatial database of annual MEOF abundance (2016-2023) across western South Dakota (SD) at 10 m spatial resolution by applying a generalized prediction model on Sentinel-2 imagery. We collected *in situ* quadrat-based total vegetation cover with MEOF percent cover estimates across western SD from 2021 through 2023 and synthesized with other available percent cover estimates (2016-2022) of several federal, state, and non-governmental sources. We conducted drone overflights at 14 sites across Butte County, SD in 2023 to develop very high spatial resolution (4-6 cm) and accurate MEOF cover maps by applying a random forest (RF) classification model. The field-measured and uncrewed aerial system (UAS) derived MEOF percent cover estimates were used to train, test, and validate a RF regression model. The predicted MEOF percent cover dataset was validated with UAS-derived percent cover in 2023 across four sites (out of 14 sites). We found that the variation in the Tasseled Cap Greenness and Normalized Difference Yellowness Index were among the top predicting variables in predicting MEOF abundance. Our predictive model yielded greater accuracies with an R^2 of 0.76, RMSE of 15.11%, MAE of 10.95%, and MAPE of 1.06%. We validated our 2023 predicted maps using the 3-m resolution PlanetScope imagery for regions where field samples could not be collected in 2023. The database of MEOF abundance showed consecutive years of average or above-average precipitation yielded a higher MEOF abundance across the study region. The database could assist local land managers and government officials pinpoint locations requiring timely land management to control the rapid spread of MEOF in the Northern Great Plains. The developed invasive MEOF percent cover datasets are freely available at the figshare repository (https://doi.org/10.6084/m9.figshare.29270759.v1).

Keywords: Invasive, UAV, random forest, Planet imagery,

https://doi.org/10.5194/essd-2025-353
Preprint. Discussion started: 4 August 2025

1. Introduction

Invasive plant species pose severe threat on ecosystem services, functioning, and structure (Rai and Singh, 2020). In particular, the Northern Great Plains (NGP) grasslands are being threatened by long-established and newly arrived invasive plant species and loss of diversity (Hendrickson et al., 2019). These invasive species compete against native species, diminishing ecological goods and services and degrading vulnerable grassland ecosystems (Gaskin et al., 2021). Furthermore, the ecosystem responses of grasslands in general including NGP are becoming increasingly variable in space and time due to the myriad influences from climate change (Bernath-Plaisted et al., 2023; Cleland et al., 2013; Zhang et al., 2022). These conditions accelerate and contribute to the difficult to predict dynamics of invasive plant species that often are spread unintentionally (Spiess et al., 2020). The NGP comprises public, tribal, and private lands, resulting in a patchwork of management goals and invasive plant control strategies (Langholz, 2010). Ecological studies that operate within restricted spatial boundaries or plot-based datasets are advantageous in providing comprehensive insights into local invasion scenarios (Martins et al., 2016). However, previous studies often miss important data, making it hard to understand invasion processes that happen continuously over space and time (Larson et al., 2020). Developing timely updates of the spatial and temporal spread of invasive plant species therefore have been increasingly suggested to effectively and efficiently address the challenges posed by invasive species in changing habitats is an urgent need (Van Rees et al., 2022).

In general, understanding spatio-temporal patterns of a biennial plant species that are either ephemeral in nature or blooms in specific years is challenging due to their phenological cycle. One such case we have for an invasive plant named yellow sweetclover (*Melilotus officinalis* (L.) Lam., MEOF) across the Northern Great Plains. There has been little to no literature on mapping blooms of such plant species till the previous decade. In recent years, MEOF has attracted attention from land managers in South Dakota (SD) as it is becoming a prominent invasive species in the NGP region. MEOF is a nitrogen-fixing, biennial legume forb native to Eurasia (Luo et al., 2016). It has noticeable pea-like, strongly scented yellow flowers arranged in a narrow raceme, which can grow more than 4 cm long (Varner, 2022). The ability of MEOF to establish and grow in a wide range of temperature, precipitation, and soil conditions has naturalized its presence in the NGP region (Kan et al., 2023). It is often one of the first plants to appear in disturbed or open sites, including pastures, agricultural fields, roadsides, rangelands, and open slopes in badlands, prairies, or floodplains (Wolf et al., 2003).

Invasive forbs such as MEOF develop inflorescences with yellow flowers that are prominent during flowering time and can be detected using 10 m resolution Sentinel-2 derived reflectance and quantitative indices (Saraf et al., 2023). Previous studies have shown that multi-temporal analysis using remote sensing data can be a powerful tool for addressing challenges in monitoring invasive species dynamics. Sentinel-2 imagery with 10 m spatial resolution has sufficed for mapping a range of invasive plant species (Kattenborn et al., 2019). In addition, the high temporal resolution of the Sentinel-2 can help capture phenological information and identify species with pronounced flowering periods. However, there have been relatively very few efforts to map MEOF in the NGP due, in part, to its unreliable annual aboveground establishment resulting in low to moderate abundance during drier years complicating attempts to map its

https://doi.org/10.5194/essd-2025-353
Preprint. Discussion started: 4 August 2025

distribution. Moreover, its yellow flowers can be easily mistaken for other yellow-flowered forbs such as yellow salsify, black eyed susan, western wallflower, annual sunflower or leafy spurge. MEOF tends to grow in dense patches and invade vast areas with the capability of growing up to 2 m tall when ample moisture is available during its growth period. In the recent wet year of 2019, MEOF thrived across the NGP, resulting in minimal spatial overlap with other yellow flowered plants and enabling researchers to map its spatial distribution. Specific years with an enhanced bloom of MEOF, such as 2019 and 2023, were easily distinguished in image time series due to their extensive spread, tall canopy, and prolific yellow flowers during summer (Preston et al., 2023). Such climate conditions create an opportunity to collect more ground samples to increase accurate mapping of MEOF distribution.

In traditional remote sensing, *in situ* reference data are required to detect and validate complex patterns and ecologically relevant processes (Mayr et al., 2019). The reference data collection is usually labor-intensive, time-consuming, and logistically difficult across large spatial areas. Uncrewed Aerial Systems (UAS), combined with high-resolution multispectral or hyperspectral cameras, offer an interesting, user-friendly, and low-cost alternative data source to *in situ* data collection (Horstrand et al., 2019; Li and Tsai, 2017; Rakotoarivony et al., 2023). Despite the limited spatial extent of each swatch, UAS still enables the acquisition of spatially continuous information on species cover with ultra-high spatial resolution (Ground Sampling Distance of <10 cm) and temporal flexibility (Turner and Wallace, 2013). Numerous studies have demonstrated the potentials of UAS data as an alternative source to supplement or even replace the traditional sampling methods of detecting species presence in the field (Alvarez-Taboada et al., 2017; Baena et al., 2017; Kattenborn et al., 2019). UAS data can be used to train models that employ fine-to-medium spatial resolution data, such as Sentinel-2 imagery, to map invasives at regional scales (Preston et al., 2023), despite a small survey extent (Colomina and Molina, 2014).

Previously, we lacked sufficient statistical power and comprehensive spatial coverage due to small sample size to conduct regional scale mapping for the 2019 MEOF blooms (Saraf et al., 2023). Preston et al., (2023) used an ensemble of MaxEnt models to map MEOF fractional cover for 2019 using UAS data from 16 sites spread across three counties in SD and Montana using satellite imagery trained from regional UAS imageries. Our team also examined the contribution of various biophysical factors to MEOF and tested different machine learning algorithms to determine the best approach to map the MEOF for 2019 (Saraf et al., 2023). We found that the random forest (RF) model outperformed other machine learning algorithms in mapping the distribution of invasive MEOF cover. However, our results indicated a significant underestimation of the percent cover due to the limited sample size. We, therefore, aimed to increase the sampling size by collecting quadrat-based percent cover and UAS imagery over MEOF blooms and synthesizing estimates from various state and federal sources to overcome uncertainties and the limitation of underestimation.

We attempted to optimize the utilization of UAS and Sentinel-2 data to create a reference percent cover dataset, which was then used as a training and validation inputs for a RF modeling framework. This approach helped develop an annual time-series percent cover database for the

https://doi.org/10.5194/essd-2025-353
Preprint. Discussion started: 4 August 2025

invasive MEOF. Developing a generalized model enables efficient mapping of irruptive invasive plant species that blooms episodically, often found in clustered patches with poor representation in the field data. Effective Management of plant invasives such as MEOF will require spatially continuous, multitemporal maps of species occurrence and cover as its first step. Building such a database for invasive MEOF can help to comprehend the spatial and temporal dynamics of its invasion patterns (Müllerová et al., 2017). Therefore, our objectives are threefold: (1) to develop a generalized prediction model using field-collected and UAS-derived percent cover samples to map the extent of invasive MEOF using Sentinel 2 imagery across western SD; (2) to compare and validate our model-derived percent cover estimates against the drone-derived estimates; and (3) to validate the predicted yellow sweetclover maps independently using PlanetScope imagery. We ask two research questions. First, what are the spatiotemporal distributions of invasive MEOF across western SD? Second, are the spatiotemporal distributions of MEOF explained by precipitation in bloom years? For land managers, it is crucial to both understand the current distribution of MEOF in recent years and appreciate its invasion dynamics, to curb further spread of MEOF into previously unaffected areas. The developed invasive species cover database would therefore, help to design mitigation strategies effectively and promote the proactive conservation of grassland ecosystems.

2. Methods

2.1 Study Area

Western SD is located within the Upper Missouri River Basin and is a part of the NGP, characterized by the Black Hills along with prairie at the southwestern corner, along with high buttes, canyons, and wide expanses of nearly level tablelands (Figure 1). This region experiences a semi-arid climate with high interannual variability in precipitation, averaging around 300-400 mm (Agnew et al., 1986). About three-fourths of the rainfall occurs during summer, and snowfall ranges from 650 mm to 5000 mm throughout western SD (Paul et al., 2016). Despite the substantial conversions of rangeland to cultivated lands in the U.S. Midwest, most of the central and western SD landscapes are still dominated by rangelands. The landscape of western SD is a mosaic of mixed-grass prairie interspersed with shrubs. The mixed grass prairie shifts into shortgrass and sagebrush grassland in the extreme western portion of the state. The dominant grasses include western wheatgrass (*Pascopyrum smithii* (Rydb.) Á. Löve), needle and thread (*Hesperostipa comata (Trin. & Rupr.)* Barkworth), little bluestem (*Schizachyrium scoparium* (Michx.) Nash), prairie sandreed (*Calamovilfa longifolia* (Hook.) Scribn), green needlegrass (*Nassella viridula (Trin.) Barkworth*), blue grama (*Bouteloua gracilis* (Willd. ex Kunth.) Lag. ex Griffiths) and threadleaf sedge (*Carex filifolia* Nutt.). Dryland sedges (*Carex spp.* L.), prairie threeawn (*Aristida oligantha* Michx.), and fringed sagewort (*Artemisia frigida* Willd.) increase with disturbance. Several perennial forbs such as western wallflower (*Erysimum asperum* (Nutt.) *DC.*), Canada thistle (*Cirsium arvense* (L.) Scop.)), leafy spurge (*Euphorbia esula* L.), purple prairie clover (*Dalea purpurea* Vent. var. *purpurea*) and shrubs such as big sagebrush (*Artemisia tridentata* Nutt.), broom snakeweed (*Gutuerrezia sorothrae* Pursh) and leadplant (*Amorpha canescens* Pursh) are prevalent. The most common invasive grasses include Kentucky bluegrass (*Poa pratensis* L.), smooth brome (*Bromus inermis* Leyss.), cheatgrass (*Bromus tectorum* L.), and curlycup gumweed (*Grindelia squarrosa (Pursh)* Dunal). Yellow salsify (*Tragopogon dubius*

https://doi.org/10.5194/essd-2025-353
Preprint. Discussion started: 4 August 2025

Scop.) and yellow sweetclover (*Melilotus officinalis* (L.) Lam.) are common invasive annual-biennial forbs in this region (Johnson and Larson, 1999).

2.2 UAS Survey

Ultra-high spatial resolution UAS imagery were acquired at 14 sites during a field campaign from July 9 to July 15, 2023. The flight locations were randomly selected across Butte County in western SD based on the availability of the larger patches of MEOF. We collected multispectral (Visible, RedEdge, and Near InfraRed) imagery using a MicaSense RedEdge-MX (MicaSense, 2015) camera deployed on a DJI Matrice 200 UAS platform. The radiometric calibration of the sensor was implemented by converting the digital values of the orthomosaic to the values of surface spectral reflectance by Micasense calibration panel. The area covered for each flight ranged between 1 ha and 10 ha, depending on the patch size of the MEOF invasion (Table S7). The imagery was captured with at least 80% forward and 75% side overlap (Table 1). We flew the flight at an average altitude of 30-60 m above ground, ensuring a spatial resolution of at least 3 cm. We used the recorded inertial measuring unit (IMU) and Global Navigation Satellite System (GNSS) module of the UAS along with Real-Time Kinematic (RTK) positioning (~1 cm accuracy) to guide the drone by placing four Ground Control Points (GCPs) at each site to ensure the geometric accuracy of the images taken by the drone matched the Sentinel-2 imagery. Several studies have demonstrated that using GCPs can lead to higher accuracies in the processed orthoimages than direct georeferencing (Jurjević et al., 2020; Padró et al., 2019). Moreover, GCPs help advance the upscaling of UAS to Sentinel-2 imagery with the best alignment and minimum shift (Gränzig et al., 2021). Therefore, we processed UAS images in Pix4D mapper (Pix4D S.A., 2022), and georeferenced the orthomosaics using the GPS coordinates of plot center and corner targets collected with Trimble Catalyst DA2 GNSS receiver kit (Trimble Inc. (n.d.), 2025) with a precision level of 1 cm accuracy. Out of the 14 sampling sites, ten sites were selected for training a random forest (RF) model; whereas, the other four were reserved for model validation.

2.3 Field measurements and sample collection

We conducted multiple field surveys during peak blooming months (June-July-August) across western SD rangelands from 2021 to 2023 (Table S1). We implemented a conventional plot-based quadrat method to estimate percent cover by averaging the grids occupied with MEOF. A minimum of three samples were collected within a 30 m × 30 m plot using 0.5 m × 0.5 m quadrats (John et al., 2018). For 2023, the GPS locations of the field-collected quadrat samples were utilized as the ground control points for enhancing the processing of drone imagery to derive percent cover samples. We retrieved 17,689 MEOF cover samples from several federal, state, and non-governmental sources for 2016-2022 across four states: South Dakota, North Dakota, Montana, and Wyoming (Figure 1a), as described in Table S1. The samples' source, year-wise distribution, and frequency distribution are given in Tables S2 and S3.

2.4 UAS derived yellow sweetclover cover

MEOF is prominently visible in orthomosaics using a combination of green, green, and blue bands. This prominence occurs because yellow flowers of MEOF increase reflectance of green while slightly decreasing reflectance of blue color (Sulik and Long, 2016). We first visually delineated several polygons of MEOF on the georeferenced orthomosaics using these band combinations. We then used 3000 absence and 3000 presence samples derived from these polygons to train a machine learning classification model and classify MEOF presence pixels

https://doi.org/10.5194/essd-2025-353
Preprint. Discussion started: 4 August 2025

from other land cover pixels. We used five spectral bands (Blue, Green, Red, RedEdge, and NIR) and the Normalized Difference Yellowness Index (NDYI) to classify the yellow-flowered blooms in the imagery. The equation for NDYI is provided in Table S4. We implemented an RF classification model on randomly split 80:20 ratio samples to segregate MEOF pixels from other pixels. We implemented hyperparameter tuning (mtry = 4 and ntrees = 1500) and 10-fold 5-repeat classification to tune the model. We tested model efficiency through visual interpretation using green-green-blue false color composites along with model metrics such as Overall Accuracy and Kappa coefficient (Landis and Koch, 1977). The binary classified MEOF present pixels were assigned with the value of 1 for present pixels and 0 for MEOF absence. We calculated the area-based weighted average of MEOF classified pixels from the total number of pixels within a 10m pixel to derive MEOF percent cover at 10 m resolution. The percent cover of MEOF within each 10 m resolution pixel was calculated as the proportion of classified MEOF pixels within that 10 m area.

We collected and averaged three field samples per 30 m × 30 m plot at each drone site in 2023. Overall, we had 30 observed percent cover samples collected across 14 drone sites. We employed a jackknife resampling procedure using leave-one-out cross-validation to calibrate RF classification-derived percent cover estimates of MEOF against field-observed percent cover values. For each iteration, one observation was excluded from the dataset, and a linear regression model was fitted using the remaining field samples. The excluded observation's field cover was then predicted using the fitted model, based solely on its derived cover value. This process was repeated for all observations, resulting in a set of cross-validated predictions for the entire dataset. Calibration accuracy was assessed by comparing predicted and observed values using root mean square error (RMSE) and the correlation coefficient of determination (R^2). We calibrated the derived percent cover values using the calibrated samples. This jackknifing approach provides an unbiased estimate of model performance and accounts for overfitting, ensuring that each prediction is made independently of the observation being predicted (Wolter, 2007).

We combined the MEOF samples collected in the field from 2016-2022 with UAS-derived 5283 samples from 2023, resulting in a total of 22,972 samples. We removed the duplicate samples from different sources falling within the same pixel location for the same year. After removing the duplicates, we had 20275 sample points. We calculated the Global Moran's I to estimate the spatial autocorrelation between the samples within each year. Due to high positive spatial autocorrelation for samples in 2019, we removed samples within a 50 m distance for 2019 and used the remaining 11,235 samples for the random forest regression model.

2.5 Satellite-derived predictor variables

We obtained 64 predictor variables with spatial resolutions ranging between 10 m and 1 km. We derived maximum value composites of various indices and tasseled caps for the peak summer months with a maximum of 10% cloud cover to enhance the spectral information of the Sentinel 2A imagery (Table S4) (Gascon et al., 2017). We also derived the coefficient of variation (standard deviation/mean) composites to represent the variability of the indices or the tasseled cap components across the summer months. For variables affected by high cloud cover or limited image availability in the seasonal composites, we used the standard deviation as an alternative to the coefficient of variation.

https://doi.org/10.5194/essd-2025-353
Preprint. Discussion started: 4 August 2025

For climate predictors, we derived mean annual and biennial total precipitation (MAP and MAP2) and temperature (MAT and MAT2) from the Daymet dataset (Version 4R1) available at 1 km spatial resolution (Thornton et al., 2022). We also computed seasonal composites (Mar+Apr+May and Jun+Jul+Aug) for total precipitation (P_{MAM} and P_{JJA}) and mean temperature (T_{MAM} and T_{JJA}). We acquired percent snow cover at 500m resolution from the MODerate resolution Imaging Spectroradiometer (MODIS) MOD10A1 V6.1 snow cover product (Riggs et al., 2015). Snow depth and snow water equivalent were acquired at 1 km spatial resolution from NOAA National Weather Service's SNOw Data Assimilation System (SNODAS) (Barrett, 2004). We computed mean composites for all snow variables during the winter (Dec+Jan+Feb).

For soil properties, we obtained soil pH, texture (sand, silt, clay, and bulk density), volumetric water content, saturated water content, and soil organic matter from the Polaris database (Chaney et al., 2019) available at 30 m resolution. For terrain features such as elevation, slope, aspect, hill shade, terrain wetness index, and terrain roughness index, we used the National Elevation Dataset from the NASA Earthdata portal available at 10 m resolution. We used a land cover/use map to mask out non-rangeland areas before implementing the regression model to emphasize the habitat of MEOF in the western SD rangelands. The land cover/use data and the proximity to roads were derived at 30 m resolution from the 2019 National Land Cover Database (NLCD 2019, Dewitz, 2021). Lastly, the distance to stream product was derived from the national hydrography dataset developed by the U.S. Geological Survey National Geospatial Program. All the variables were acquired from the Google Earth Engine (GEE) platform and processed in ArcMap 10.8.1. All variables were resampled to 10 m resolution and projected in Albers Equal Area projection and WGS 84 datum. A detailed summary of all the independent variables utilized in this study is provided in Table S5. The method workflow for predicting the invasive yellow sweetclover percent cover for 2016-2023 is illustrated in Figure 2.

2.6 MEOF cover regression model

Most machine learning models such as RFs works on the assumption that the samples are independent and identically distributed. If this assumption is violated due to spatial autocorrelation, model performance metrics (like accuracy, R^2) can be overestimated (Liu et al., 2022). To deal with this issue, we calculated Global Moran's I with a minimum distance of 50 m on the MEOF percent cover samples to test for spatial autocorrelation between the samples within each year (Moran, 1950). We implemented permutation test for the samples to generate the null distribution and assess the significance of the Moran's I. A 50 m threshold is equivalent to five pixels which helps in mitigating the influence of immediate neighbors, which often exhibit strong spatial autocorrelation due to their proximity. By setting this distance, we aimed at reducing local clustering and ensuring a degree of spatial independence among samples, which is critical for robust estimation of global spatial autocorrelation. Similar buffer distances have been used in previous ecological studies to distinguish between fine-scale spatial dependence and broader spatial patterns, particularly in heterogeneous landscapes where plant cover could be spatially clustered at short ranges (Baumann et al., 2025). We removed the spatially-correlated samples and later used 11,235 observed samples to develop a generalized percent cover regression model using the *Random Forest* algorithm (Breiman et al., 1984). We overlaid these observed samples on predictor variable (rasters) to derive a predictor variable database for training an RF model. We implemented a spearman correlation coefficient (r) threshold of 0.8 to

https://doi.org/10.5194/essd-2025-353
Preprint. Discussion started: 4 August 2025

remove highly correlated predictor variables (Dubuis et al., 2011; Stohlgren et al., 2010; Zar, 2005). We then implemented a Recursive Feature Elimination (RFE) method with 5-repeat, 10-fold cross-validation to determine the top predicting variables (Breiman, 2017; Guyon et al., 2002). The observation samples were split in an 80:20 ratio for training and testing sets using the bootstrap method with replacement. All the variables were scaled and centered before the development of the prediction model. We implemented hyperparameter tuning (*mtry* and *ntrees)* and used the mean absolute error (MAE), mean absolute percentage error (MAPE), root mean square error (RMSE), and the coefficient of determination (R^2) metrics to evaluate the model performance during the testing phase. The MEOF percent cover was predicted using the best generalized model and the best statistical metrics. We used the reference of the habitat suitability map from Saraf et al., (2023) to mask out the low probability of occurrence regions and to develop final MEOF prediction maps. All the analyses were performed using the 'caret' package in the RStudio environment (Kuhn, 2015).

3. Results

3.1 Yellow sweetclover cover from UAS imagery

We used 6,000 training points to train and test an RF classification model by splitting them to an 80:20 ratio, obtaining 4,795 training and 1,205 testing samples. The developed RF classification model exhibited an overall accuracy of 98.76% and kappa of 0.97 in distinguishing MEOF pixels. The confusion matrix for the classification model is provided in Table S6. The RF classification accuracies can be visually validated in three exemplary UAS sites with MEOF blooms. Figure 3 shows the three UAS training sites with (a) UAS orthoimage with green, green, and blue band combination, (b) NDYI with darker brown representing MEOF presence, (c) RF classified image showing MEOF presence, and (d) the derived MEOF percent cover at 10 m pixel resolution. The estimated area covered with the classified MEOF presence pixels derived from the RF classification model can be found in Table S7. We generated 5,283 percent cover samples from UAS, which were divided into 2,736 samples for training sites and the remaining 2,547 samples for validating the RF regression model. The samples were segregated based on ten training and four validation locations. We implemented the jackknifing to calibrate the derived MEOF cover. The cross-validated predictions showed good agreement with the field observed samples with the R^2 of 0.68 and RMSE of 6.24%, suggesting relatively low average prediction error.

3.2 Random Forest predictions

We used the spearman correlation test (r) on all 64 independent variables with a threshold of 0.8 and selected 25 predictor variables (Figure S1). We later implemented a recursive feature selection on the 25 predictor variables and selected the 13 top predictor variables (Table 2). We took the threshold of 0.3 for Moran's I to reduce the positive spatial autocorrelation among the samples. We used sampling with replacement to calculate the significance of the Moran's I. We found that all the years except 2019 and 2023 showed very low spatial autocorrelation with Moran's I of <0.2 (Table S8). We reduced the spatially autocorrelated samples for 2019 and 2023 by selecting samples beyond a minimum distance of 50 m. Overall, we used a total of 11,235 training samples to develop an RF model to predict invasive MEOF cover across western SD. We used 80% of these samples (9,006 samples) for training and 20% (2,229 samples) for testing the model, with 3 *mtry* and 1500 *ntrees* as the optimized hyperparameters for the regression model. We noticed that the reduction in sample size had little-to-no effect on the

https://doi.org/10.5194/essd-2025-353
Preprint. Discussion started: 4 August 2025

model statistics and metrices. The developed RF model exhibited an R^2 of 0.76, RMSE of 15.11, MAE of 10.95, and MAPE of 1.06 %. The predicted cover maps for 2019 and 2023 showed a relatively higher percent cover range than those for other years (Figure S2). The temporal maps showed a higher cover of MEOF in the western counties compared to the eastern counties of western SD (Figure 4). We also found that the MEOF cover followed moisture gradients as higher cover was evident near floodplains. We also found that the western section of the study region, including Butte, Harding, Pennington, Custer, and Fall River counties, were the major hotspots for MEOF cover and showed persistent higher percent cover particularly in 2018, 2019 and 2023. This region tends to have a broader spread of high-density cover over the years. The hotspots were more evident in wet years especially along the floodplains of the Missouri River tributaries, as we move along the west-to-east gradient across western SD. Variable importance showed Normalized Difference Moisture Index (NDMI), proximity to roads (Dist_roads), variability in Normalized Difference Water Index (NDWIcv), and Elevation were the top contributing variables for predicting MEOF cover (Figure S3).

4. Discussion

4.1 Significance of mapping MEOF blooms

We refer to those years with mass blooming of MEOF in the Dakota region as "sweetclover years". They occurred only during wetter years, when mass blooming cover followed higher than average precipitation (Gucker, 2009). However, climate variables like annual precipitation or snow depth, did not rank among the top predicting variables. This unexpected result may be due to the large disparity in spatial resolution between Sentinel-derived variables at 10 m and the 1 km climate variables, with the 10,000-fold difference in spatial resolution contributing to an underestimation of precipitation as a significant variable. Therefore, we created a MEOF percent cover map series for 2016 through 2023 and compared it with precipitation anomaly maps during the same period computed using the Daymet dataset product. These precipitation anomaly maps showed that the western SD witnessed above-average precipitation in a few regions for 2018 and 2023 and most of the western SD for 2019 (Figure S4). The central and eastern counties in 2019 and central and southern counties in 2023 showed a greater range of MEOF covers showing consistent pattern of MEOF resurgence with the return of wet conditions. Despite 2016 being relatively normal or slightly dry year, sweetclover cover remained moderate with less spatial variability, indicating less widespread establishment. The widespread establishment of MEOF could be seen increasing in 2018 with high CV of 0.5 and then its percent cover reached a peak in the subsequent year of 2019. For the years 2020, 2021 and 2022, most regions experienced average to below-average rainfall conditions. During these years, MEOF percent cover reached up to 50%, with the sharp drop in percent cover in 2021, where the maximum cover was only 43%. This showed drought conditions likely limit growth and establishment. The year 2020 and 2022 acted as transitional years, possible due to lagged ecological response. For dry years, the majority of western SD predicted less than 50% cover.

Overall, we found a high percent cover range in the western counties of western SD including Butte, Meade, Pennington, Custer, Fall River, Jackson, Bennet and Oglala Lakota counties. Central regions showed fluctuating trends with moderate to high coverage in some years (e.g., 2018, 2019, 2023) and relatively low in other years (e.g., 2020, 2021). In the eastern counties (i.e., Corson, Dewey, and Stanley), we observed a relatively low percent cover range with <20%. In this region, MEOF appeared to be more scattered and patchier with some local increases near

https://doi.org/10.5194/essd-2025-353
Preprint. Discussion started: 4 August 2025

floodplains, which are situated at lower elevations and benefit from high moisture availability especially in the years 2018 and 2019. Nevertheless, despite experiencing ample moisture in some areas in 2016 or 2018, the 'sweetclover year' mass blooming was limited only to 2019. This phenomenon may be attributed to MEOF's biennial life cycle, which plays a significant role and acts as a lag effect provided average or above average conditions persist. A distinct drop in coverage is seen in the years of 2020 and 2021 across the south, with recovery in 2022–2023. During the summer fieldwork of 2022, we observed MEOF predominantly in the first year of its life cycle and an ample cover of MEOF blooms in the Butte County in the consecutive year, in huge patches to be captured by the drones. This temporal pattern arises from the biennial growth period of MEOF. Moreover, MEOF with >40% percent cover was found in mostly regions that received above-average precipitation during both dry and wet years. Though the RF model did not identify precipitation as the top variable, time-series precipitation maps supported the hypothesis that 'sweetclover years' characterized by high MEOF abundance may occur when sustained average or above-average precipitation conditions help maintain sufficient soil moisture levels, despite losses from evapotranspiration. These favorable moisture conditions likely facilitate the successful establishment and dominance of MEOF across the Northern Great Plains rangelands. Additionally, we predicted MEOF percent cover estimates for the year 2024 using our trained model (Figure S5). However, this 2024 predictions has not yet been validated due to the unavailability of field data. Validation of model performance for 2024 and subsequent years remains a key focus for future work.

Our study offers a workflow for different plant species of annuals, biennials, or geophytes that share dominance during the blooming events, displaying huge appearances in specific years with differences of 4 to 10 weeks in their length and peak of the flowering period (Vidiella et al., 1999). These blooms cause a sudden increase in annual net primary production, triggering relevant changes in the ecosystem such as soil nitrogen content, temporary plant composition modifications, attraction of predators, etc. (Jaksic, 2001), as well as changes in the local climate: an increase in evapotranspiration and a decrease in albedo (He et al., 2017). Various bloom events in arid and semi-arid regions, such as rare blooms in the arid Atacama Desert or superblooms of wildflowers in California's southeastern deserts, have fascinated many researchers and media sources recently (Chávez et al., 2019; Martínez-Harms et al., 2022; Winkler and Brooks, 2020). Our workflow could be useful for detecting and monitoring such events, as well as for managing invasive plant species in grassland ecosystems. Effective management strategies can help mitigate the impact of these invasive species, promoting the health and resilience of grassland ecosystems.

The comprehensive database developed for the invasive MEOF provides a critical foundation for understanding its spatial-temporal invasion dynamics across western SD. The database facilitates detailed analyses of spread dynamics, invasion pathways, and distributional hotspots, thereby improving the ability to model present distribution patterns and project future range expansions under diverse environmental conditions. It also offers a valuable resource for long-term ecological monitoring and adaptive management of MEOF. Furthermore, the dataset supports investigations into the ecological consequences of invasion, including potential associations between MEOF cover and declines in native species richness, particularly within nitrogen-limited prairie ecosystems. Beyond immediate applications, this database contributes to a

https://doi.org/10.5194/essd-2025-353
Preprint. Discussion started: 4 August 2025

broader understanding of community-level vegetation changes driven by nitrogen-fixing invasive species in grassland environments.

4.2 Significance of predictor variables

The variable importance results for MEOF reveals that Normalized Difference Moisture Index (NDMI) is the most influential predictor, indicating that soil and vegetation moisture plays a crucial role in supporting its invasion and growth (Figure S2). NDMI characterizes the water stress level in plants (Gao, 1996), which has been used to monitor drought stress and vegetation moisture content (Strashok et al., 2022). Proximity to roads (Dist_roads) emerged as the second most important predictor, explaining the higher cover of MEOF near the roads and its dispersion through road corridors, as MEOF was previously planted along roadsides for soil stabilization (Gucker, 2009). These findings align well with those of Wurtz et al., (2010) who showed that MEOF might have spread onto floodplains from roads, mines, and agricultural fields. We also found variability in Normalized Difference Water Index (NDWIcv) indicating areas with fluctuating surface water availability may create favourable conditions for MEOF establishment. Furthermore, most climatic variables, such as snow depth, variability in snow depth, mean annual precipitation and Temperature (MAP and MAT), and variability in mean annual precipitation (MAPcv), were found to be of relatively low importance, likely because of their coarser spatial resolutions (500 m and 1 km). It could also suggest that climate may set the broad suitability for MEOF but local moisture dynamics and human disturbances may play more critical role in shaping MEOF invasion patterns.

4.3 MEOF cover estimates for 2019

We compared our predicted MEOF cover map with those of Saraf et al., (2023) for 2019. We found that increasing the sample size and ensuring a more balanced distribution significantly improved our model accuracy, raising R^2 from 0.55 to 0.76, though it also increased RMSE. Saraf et al. (2023) noted that the model underestimated the percent cover range due to the limited sample size (n = 1,612) and the limited frequency of high percent cover observation samples. The study showed that the RF model performed adequately with R^2 of 0.55 and RMSE of 7.49, even with a limited sample size (n = 1,612). In contrast, current model utilized a larger and more balanced sample size (n = 11,235) with a uniform frequency distribution across years. The increase in sample size led to a significant improvement in model accuracy, raising R^2 but also increased RMSE from 7% to 15% due to the unbalanced sample distribution across years. This finding suggests that balanced sample sizes have the potential to improve both the prediction range and accuracy of the model, though further testing with unbalanced designs is needed to fully evaluate their efficacy.

Both predicted maps exhibited similar spatial patterns, with higher MEOF cover observed in the western SD counties, such as Butte and Pennington. However, our model predicted a full range of 0-100% cover for 2019, in contrast to the limited range observed in Saraf et al., (2023). This difference is particularly evident in the high MEOF probability areas of western SD rangelands, as shown in Figure 5.

We conclude that Saraf et al., (2023) significantly underestimated the extent of high percent cover, reporting that areas with > 50% MEOF cover constituted only about 0.76% of SD's total rangelands. In contrast, our updated prediction model estimated that ~12.6% (10,256 km²) of the

https://doi.org/10.5194/essd-2025-353
Preprint. Discussion started: 4 August 2025

total rangeland area (81,442 km²) had >50% MEOF cover in 2019. The increase in sample size improved the model ability to predict a wider range of percent cover, providing a more accurate representation of the massive MEOF blooms across western SD in 2019.

4.4 Uncertainties

We manually delineated polygons of invasive MEOF presence, which were then used to train the RF classifier. The UAS orthomosaics in a green-blue-blue band false color combination helped to delineate training polygons. This approach highlighted the potential of multi-spectral bands to easily detect MEOF patches. Furthermore, we randomly sampled 6,000 pixels at 4-6 cm resolution corresponding to the presence and absence of the invasive MEOF. It was anticipated that errors might occur during the manual delineation, although the RGB imagery employed in the study displayed the MEOF's characteristic features, such as color, canopy shape, and flowers. The reliability of visual delineation could be compromised in shaded areas. However, the RF classification could accurately distinguish most MEOF pixels from non-MEOF pixels with 98.6%. Visual inspections revealed no discrepancies between the derived percent cover maps at 10 m resolution and submeter resolution MEOF classified maps. This result suggests that any alignment errors were likely minimal and did not significantly affect model accuracy at 10 m resolution especially after calibration of the derived percent cover. While these results are specific to our study area in the Northern Great Plains, the approach has broader potential. We also produced a predictive map for the year 2024 using the trained model. Assessing the accuracy of the 2024 predictions and extending validation to upcoming future years constitutes an important direction for continued research. Our workflow combined with high-resolution UAS imagery and machine learning can be adapted to other regions with similar vegetation structure and invasion dynamics, offering a scalable and efficient tool for detecting and mapping invasive biennials like MEOF across diverse rangeland ecosystems.

4.5 Validation for 2023 estimates

We validated the predicted MEOF cover map with the remaining four UAS-validation sites and found that the predictions exhibited high correlation with the observed MEOF in the UAS imagery (Figure 6). Figure 6 shows the four validation sites in the green-green-blue false color composite along with the predicted yellow sweetclover percent cover at 10 m resolution. The validation sites showed a good correspondence between the predicted percent cover and the derived percent cover with R^2 of 0.71, RMSE of 17.81%, MAE of 13.17, and MAPE of 4.89% (Figure S6). We found that the prediction model underestimated the high percent cover range and overestimated the low to no percent cover regions. The prediction map for 2023 revealed higher cover in the western counties, such as Butte, Harding, and Pennington counties. We found that only 0.76 % (621.4 km^2) of the total rangeland area (81,442 km^2) exhibited cover above 50% in 2023. During our summer fieldwork, we observed yellow sweetclover (MEOF) cover extensive enough to be effectively captured by drone flights in these regions. MEOF has a prominent yellow flower that is distinctly visible in UAS and satellite imagery, provided the blooms appear cover in larger patches enough to be visible in the respective resolutions. Numerous previous remote sensing studies of invasive species have used binary (presence/absence) classification approaches to map invasive species (Bradley, 2014). We chose to map the MEOF on an ordinal scale as this approach offers a measure of invasion intensity at a

https://doi.org/10.5194/essd-2025-353
Preprint. Discussion started: 4 August 2025

larger landscape scale. We assert that assessing MEOF cover across the region can help better evaluate the economic and ecological impacts of this invasive plant species.

4.6 Validation with PlanetScope Imagery

We downloaded four-band (visible and near infrared), 3 m resolution Dove Classic and SuperDove PlanetScope (PS) imagery for 2019 and 2023 using our access to the NASA Commercial SmallSat Data Acquisition (CSDA) program to validate our prediction maps (Planet Labs PBC, 2023). We acquired PS scenes at four different locations with high percent cover field sample points for 2019 and high MEOF cover predicted in 2019 and 2023 percent cover maps. We again found that the false color combination of green-green-blue worked well to visualize MEOF blooms. We observed that the intensity of MEOF flowering at the full bloom stage was also discernible through PS imagery for 2019 and 2023, confirming the presence of MEOF in these selected regions during the high MEOF cover years (Figure 7). We found that each site in 2023 exhibited a similar yellow reflectance of MEOF as observed in 2019. This result confirms that our generalized model accurately predicted the presence of MEOF in sites where we did not have field samples for 2023.

4.7 Limitations

Our model does not explain the variation in the MEOF cover that has biennial life cycle. Therefore, we aimed at mapping MEOF blooms or when MEOF was at flowering stage. Most of the observed MEOF cover samples were collected during the second year of its life cycle to enable capture of its flowering stage. The yellow sweetclover cover peaked during the wetter years (2019 and 2023) as shown in Figure S3, and most of the sampling strength was obtained during these years (Table S1). We used the coefficient of variation to capture the temporal variation of the independent variables during summer (JJA). However, cloud cover above 10% in the region remained the major limitation of this study. In certain cases, we also examined the Harmonized Landsat Sentinel-2 (HLS) product (Claverie et al., 2018), where the cloud-free maximum seasonal composites were limited to a single image per season due to the scarcity of cloud-free images. We resolved this issue by substituting the coefficient of variation with the standard deviation of the seasonal mean of the variable. Sentinel-2 data provides high temporal resolution, fast data provisioning, and computing infrastructure, making it easier for land managers to track invasive species in real-time. Our model demonstrated high variable importance of high-resolution variables performed better than climate variables due to their coarser resolution. This underperformance of coarser variables suggests the need for higher spatial resolution datasets in mapping invasive plant species. High-resolution mapping with uneven spatial resolution variables also makes it more difficult to understand the relative roles of environmental variables in characterizing the niche of invasive species.

5. Data availability

The developed invasive MEOF percent cover datasets are freely available at the figshare repository (Saraf et al., 2025) (https://doi.org/10.6084/m9.figshare.29270759.v1). The repository has two folders: the first folder named “resampled predicted cover maps” contains predicted percent cover maps of invasive yellow sweetclover resampled at 20m resolution due to size limitations. We can provide the original 10m resolution images upon request. Each file is saved

https://doi.org/10.5194/essd-2025-353
Preprint. Discussion started: 4 August 2025

in GeoTiff format in the Albers Conic Equal Area projection. Each file is saved with an acronym of 'm' for MEOF followed by an underscore and a year. Missing data are represented by "No data". The other folder named "sample_code_and_data" contains the R code and an exemplary sample data to predict the MEOF percent cover.

6. Conclusions

Our integrated approach combining high-resolution UAS imagery, RF classification and regression models, and multi-year satellite and climatic data enabled the effective mapping and monitoring of MEOF cover across western South Dakota. The models demonstrated strong performance with high accuracy in both classification and regression tasks, validating the use of drone-derived percent cover for landscape-scale predictions. The findings highlight the critical role of local moisture availability, proximity to roads, and surface water variability in driving MEOF invasion, while broader climatic variables played a comparatively limited role due to their coarser resolution. Temporal maps revealed that MEOF expansion is closely linked to wetter years, aligning with its biennial life cycle and reinforcing the concept of "sweetclover years." The updated 2019 cover map was significantly improved from the previous estimates, capturing a broader percent cover range and representing invasion hotspots. Validation using 2023 UAS sites and PlanetScope imagery further confirmed the model's reliability. Our study proposes a workflow of a generalized model that could be applicable to various plant species annuals, biennials, and geophytes that exhibit episodic dominance during blooming events. Our database on MEOF enables analysis of its invasion dynamics, supports predictive modeling of current and future distributions, and informs long-term monitoring and management. It also provides a foundation for assessing ecological impacts on native species and community composition in nitrogen-poor grasslands. Our study also provides a valuable tool for detecting and monitoring irruptive blooming events and can support the management of invasive plant species such as MEOF in grassland ecosystems. Effective management strategies informed by these insights may help mitigate the ecological impacts of invasive species, thereby enhancing the health and resilience of grassland environments.

Code availability

The codes used to produce the multitemporal MEOF maps are publicly available on figshare repository (Saraf et al., 2025) (https://doi.org/10.6084/m9.figshare.29270759.v1).

Author contributions

SS – Conceptualization, Data Curation, Formal Analysis, Methodology, Software, Validation, Visualization, and Writing – original draft, review & editing. RJ - Funding acquisition, Project administration, Resources, Supervision, Conceptualization and Writing – review & editing. VK – Data Curation, Visualization, Software, Writing – review & editing. KJ - Data Curation, Writing – review & editing. GH - Visualization, Writing – review & editing. JC - Writing – review & editing. RL - Writing – review & editing.

Acknowledgements

We thank all the institutes, organizations, and developers of the various datasets for making their products freely available. Our appreciation also goes to NASA Commercial SmallSat Data

https://doi.org/10.5194/essd-2025-353
Preprint. Discussion started: 4 August 2025

Acquisition (CSDA) program for providing us access with PlanetScope Imagery. We would also like to thank Michele Thornton for providing us Daymet data for 2024 way ahead of its release for us to predict MEOF percent cover for 2024.

Competing interests

The contact author has declared that none of the authors has any competing interests.

References

Agnew, W., Uresk, D. W., and Hansen, R. M.: Flora and Fauna Associated with Prairie Dog Colonies and Adjacent Ungrazed Mixed-grass Prairie in Western South Dakota, https://doi.org/10.2307/3899285, 1986.

Alvarez-Taboada, F., Araújo-Paredes, C., and Julián-Pelaz, J.: Mapping of the Invasive Species Hakea sericea Using Unmanned Aerial Vehicle (UAV) and WorldView-2 Imagery and an Object-Oriented Approach, Remote Sens., 9, 913, https://doi.org/10.3390/rs9090913, 2017.

Baena, S., Moat, J., Whaley, O., and Boyd, D.: Identifying species from the air: UAVs and the very high resolution challenge for plant conservation, PLoS One, 12, e0188714, https://doi.org/10.1371/journal.pone.0188714, 2017.

Barrett, B.: Snow Data Assimilation System (SNODAS) Data Products at NSIDC, Version 1, Center, Natl. Oper. Hydrol. Remote Sens., https://doi.org/10.7265/N5TB14TC, 2004.

Baumann, E., Beierkuhnlein, C., Preitauer, A., Schmid, K., and Rudner, M.: Evaluating remote sensing data as a tool to minimize spatial autocorrelation in in-situ vegetation sampling, Erdkunde, 79, 25–40, https://doi.org/10.3112/erdkunde.2025.01.02, 2025.

Bernath-Plaisted, J. S., Ribic, C. A., Hills, W. B., Townsend, P. A., and Zuckerberg, B.: Microclimate complexity in temperate grasslands: implications for conservation and management under climate change, Environ. Res. Lett., 18, https://doi.org/10.1088/1748-9326/acd4d3, 2023.

Bradley, B. A.: Remote detection of invasive plants: A review of spectral, textural and phenological approaches, Biol. Invasions, 16, 1411–1425, https://doi.org/10.1007/s10530-013-0578-9, 2014.

Breiman, L.: Classification and regression trees, Routledge, 2017.

Breiman, L., Friedman, J. H., Olshen, R. A., and Stone, C. .: Classification And Regression Trees (1st ed.), Routledge, https://doi.org/https://doi.org/10.1201/9781315139470, 1984.

Chaney, N. W., Minasny, B., Herman, J. D., Nauman, T. W., Brungard, C. W., Morgan, C. L. S., McBratney, A. B., Wood, E. F., and Yimam, Y.: POLARIS Soil Properties: 30-m Probabilistic Maps of Soil Properties Over the Contiguous United States, Water Resour. Res., 55, 2916–2938, https://doi.org/10.1029/2018WR022797, 2019.

Chávez, R. O., Moreira-Muñoz, A., Galleguillos, M., Olea, M., Aguayo, J., Latín, A., Aguilera-Betti, I., Muñoz, A. A., and Manríquez, H.: GIMMS NDVI time series reveal the extent, duration, and intensity of "blooming desert" events in the hyper-arid Atacama Desert, Northern Chile, Int. J. Appl. Earth Obs. Geoinf., 76, 193–203, https://doi.org/https://doi.org/10.1016/j.jag.2018.11.013, 2019.

Claverie, M., Ju, J., Masek, J. G., Dungan, J. L., Vermote, E. F., Roger, J.-C., Skakun, S. V., and Justice, C.: The Harmonized Landsat and Sentinel-2 surface reflectance data set, Remote Sens. Environ., 219, 145–161, 2018.

Cleland, E. E., Collins, S. L., Dickson, T. L., Farrer, E. C., Gross, K. L., Gherardi, L. A., Hallett, L. M., Hobbs, R. J., Hsu, J. S., Turnbull, L., and Suding, K. N.: Sensitivity of grassland plant

https://doi.org/10.5194/essd-2025-353
Preprint. Discussion started: 4 August 2025

community composition to spatial vs. temporal variation in precipitation, Ecology, 94, 1687–1696, https://doi.org/https://doi.org/10.1890/12-1006.1, 2013.

Colomina, I. and Molina, P.: Unmanned aerial systems for photogrammetry and remote sensing: A review, ISPRS J. Photogramm. Remote Sens., 92, 79–97, https://doi.org/https://doi.org/10.1016/j.isprsjprs.2014.02.013, 2014.

Dewitz, J.: National Land Cover Database (NLCD) 2019 Products, US Geol. Surv. Sioux Falls, SD, USA, https://doi.org/https://doi.org/10.5066/P9KZCM54, 2021.

Dubuis, A., Pottier, J., Rion, V., Pellissier, L., Theurillat, J. P., and Guisan, A.: Predicting spatial patterns of plant species richness: A comparison of direct macroecological and species stacking modelling approaches, Divers. Distrib., 17, 1122–1131, https://doi.org/10.1111/j.1472-4642.2011.00792.x, 2011.

Gao, B.: NDWI—A normalized difference water index for remote sensing of vegetation liquid water from space, Remote Sens. Environ., 58, 257–266, https://doi.org/https://doi.org/10.1016/S0034-4257(96)00067-3, 1996.

Gascon, F., Bouzinac, C., Thépaut, O., Jung, M., Francesconi, B., Louis, J., Lonjou, V., Lafrance, B., Massera, S., Gaudel-Vacaresse, A., Languille, F., Alhammoud, B., Viallefont, F., Pflug, B., Bieniarz, J., Clerc, S., Pessiot, L., Trémas, T., Cadau, E., De Bonis, R., Isola, C., Martimort, P., and Fernandez, V.: Copernicus Sentinel-2A calibration and products validation status, Remote Sens., 9, https://doi.org/10.3390/rs9060584, 2017.

Gaskin, J. F., Espeland, E., Johnson, C. D., Larson, D. L., Mangold, J. M., McGee, R. A., Milner, C., Paudel, S., Pearson, D. E., Perkins, L. B., Prosser, C. W., Runyon, J. B., Sing, S. E., Sylvain, Z. A., Symstad, A. J., and Tekiela, D. R.: Managing invasive plants on Great Plains grasslands: A discussion of current challenges, Rangel. Ecol. Manag., 78, 235–249, https://doi.org/10.1016/j.rama.2020.04.003, 2021.

Gränzig, T., Fassnacht, F. E., Kleinschmit, B., and Förster, M.: Mapping the fractional coverage of the invasive shrub Ulex europaeus with multi-temporal Sentinel-2 imagery utilizing UAV orthoimages and a new spatial optimization approach, Int. J. Appl. Earth Obs. Geoinf., 96, https://doi.org/10.1016/j.jag.2020.102281, 2021.

Gucker, C. L.: Melilotus alba, M. officinalis, U.S. Dep. Agric. For. Serv. Rocky Mt. Res. Station. Fire Sci. Lab., 2009.

Guyon, I., Weston, J., Barnhill, S., and Vapnik, V.: Gene Selection for Cancer Classification using Support Vector Machines, Mach. Learn., 46, 389–422, https://doi.org/10.1023/A:1012487302797, 2002.

He, B., Huang, L., Liu, J., Wang, H., Lű, A., Jiang, W., and Chen, Z.: The observed cooling effect of desert blooms based on high-resolution Moderate Resolution Imaging Spectroradiometer products, Earth Sp. Sci., 4, 247–256, https://doi.org/https://doi.org/10.1002/2016EA000238, 2017.

Hendrickson, J. R., Sedivec, K. K., Toledo, D., and Printz, J.: Challenges Facing Grasslands inthe Northern Great Plains and North Central Region, Rangelands, 41, 23–29, https://doi.org/https://doi.org/10.1016/j.rala.2018.11.002, 2019.

Horstrand, P., Guerra, R., Rodríguez, A., Díaz, M., López, S., and López, J. F.: A UAV Platform Based on a Hyperspectral Sensor for Image Capturing and On-Board Processing, IEEE Access, 7, 66919–66938, https://doi.org/10.1109/ACCESS.2019.2913957, 2019.

Jaksic, F. M.: Ecological effects of El Niño in terrestrial ecosystems of western South America, Ecography (Cop.)., 24, 241–250, https://doi.org/https://doi.org/10.1111/j.1600-0587.2001.tb00196.x, 2001.

https://doi.org/10.5194/essd-2025-353
Preprint. Discussion started: 4 August 2025

John, R., Chen, J., Giannico, V., Park, H., Xiao, J., Shirkey, G., Ouyang, Z., Shao, C., Lafortezza, R., and Qi, J.: Grassland canopy cover and aboveground biomass in Mongolia and Inner Mongolia: Spatiotemporal estimates and controlling factors, Remote Sens. Environ., 213, 34–48, https://doi.org/10.1016/j.rse.2018.05.002, 2018.

Johnson, J. R. and Larson, G. E.: Grassland Plants of South Dakota and the Northern Great Plains, Research Bulletins of the South Dakota Agricultural Experiment Station (1887-2011), 764 pp., 1999.

Jurjević, L., Gašparović, M., Milas, A. S., and Balenović, I.: Impact of UAS Image Orientation on Accuracy of Forest Inventory Attributes, Remote Sens., 12, https://doi.org/10.3390/rs12030404, 2020.

Kan, H., Teng, W., Chen, C., Zhang, G., and Pang, Z.: Establishment of alien invasive plant, yellow sweet clover (Melilotus officinalis) at a complex ecosystem distributed with farmlands and wasted lands, https://doi.org/10.21203/rs.3.rs-2933552/v1, 2023.

Kattenborn, T., Lopatin, J., Förster, M., Braun, A. C., and Fassnacht, F. E.: UAV data as alternative to field sampling to map woody invasive species based on combined Sentinel-1 and Sentinel-2 data, Remote Sens. Environ., 227, 61–73, https://doi.org/https://doi.org/10.1016/j.rse.2019.03.025, 2019.

Kuhn, M.: A Short Introduction to the caret Package, R Found. Stat. Comput., 1–10, 2015.

Landis, J. R. and Koch, G. G.: The Measurement of Observer Agreement for Categorical Data, Biometrics, 33, 159, https://doi.org/10.2307/2529310, 1977.

Langholz, J.: Global Trends in Private Protected Areas and their Implications for the Northern Great Plains Source : Great Plains, Gt. Plains Res., 20, 9–16, 2010.

Larson, E. R., Graham, B. M., Achury, R., Coon, J. J., Daniels, M. K., Gambrell, D. K., Jonasen, K. L., King, G. D., LaRacuente, N., Perrin-Stowe, T. I. N., Reed, E. M., Rice, C. J., Ruzi, S. A., Thairu, M. W., Wilson, J. C., and Suarez, A. V: From eDNA to citizen science: emerging tools for the early detection of invasive species, Front. Ecol. Environ., 18, 194–202, https://doi.org/https://doi.org/10.1002/fee.2162, 2020.

Li, L.-Y. and Tsai, C.-C.: Accessing online learning material: Quantitative behavior patterns and their effects on motivation and learning performance, Comput. Educ., 114, https://doi.org/10.1016/j.compedu.2017.07.007, 2017.

Liu, X., Kounadi, O., and Zurita-Milla, R.: Incorporating Spatial Autocorrelation in Machine Learning Models Using Spatial Lag and Eigenvector Spatial Filtering Features, https://doi.org/10.3390/ijgi11040242, 2022.

Luo, K., Jahufer, M. Z. Z., Wu, F., Di, H., Zhang, D., Meng, X., Zhang, J., and Wang, Y.: Genotypie variation in a breeding population of yellow sweet clover (Melilotus officinalis), Front. Plant Sci., 7, 1–10, https://doi.org/10.3389/fpls.2016.00972, 2016.

Martínez-Harms, J., Guerrero, P., Martinez-Harms, M., Poblete, N., González, K., Stavenga, D., and Vorobyev, M.: Mechanisms of flower coloring and eco-evolutionary implications of massive blooming events in the Atacama Desert, Front. Ecol. Evol., 10, https://doi.org/10.3389/fevo.2022.957318, 2022.

Martins, J., Richardson, D. M., Henriques, R., Marchante, E., Marchante, H., Alves, P., Gaertner, M., Honrado, J. P., and Vicente, J. R.: A multi-scale modelling framework to guide management of plant invasions in a transboundary context, For. Ecosyst., 3, https://doi.org/10.1186/s40663-016-0073-8, 2016.

Mayr, S., Kuenzer, C., Gessner, U., Klein, I., and Rutzinger, M.: Validation of Earth Observation Time-Series: A Review for Large-Area and Temporally Dense Land Surface Products,

https://doi.org/10.5194/essd-2025-353
Preprint. Discussion started: 4 August 2025

760 Remote Sens., 11, 2616, https://doi.org/10.3390/rs11222616, 2019.
761 Moran, P. A. P.: Notes on Continuous Stochastic Phenomena, Biometrika, 37(2), 17–29, 1950.
762 Müllerová, J., Brůna, J., Bartaloš, T., Dvořák, P., Vítková, M., and Pyšek, P.: Timing Is
763 Important: Unmanned Aircraft vs. Satellite Imagery in Plant Invasion Monitoring, Front.
764 Plant Sci., 8, 1–13, https://doi.org/10.3389/fpls.2017.00887, 2017.
765 Padró, J.-C., Muñoz, F.-J., Planas, J., and Pons, X.: Comparison of four UAV georeferencing
766 methods for environmental monitoring purposes focusing on the combined use with airborne
767 and satellite remote sensing platforms, Int. J. Appl. Earth Obs. Geoinf., 75, 130–140,
768 https://doi.org/https://doi.org/10.1016/j.jag.2018.10.018, 2019.
769 Paul, M., Rajib, A., and Ahiablame, L.: Spatial and Temporal Evaluation of Hydrological
770 Response to Climate and Land Use Change in Three South Dakota Watersheds, JAWRA J.
771 Am. Water Resour. Assoc., 53, https://doi.org/10.1111/1752-1688.12483, 2016.
772 Pix4D S.A.: Pix4Dmapper. Version 4.8, www.pix4d.com, 2022.
773 Planet Labs PBC: Planet Application Program Interface: In Space for Life on Earth,
774 https://api.planet.com, 2023.
775 Preston, T. M., Johnston, A. N., Ebenhoch, K. G., and Diehl, R. H.: Beyond presence mapping:
776 predicting fractional cover of non-native vegetation in Sentinel-2 imagery using an ensemble
777 of MaxEnt models, Remote Sens. Ecol. Conserv., 9, 512–526,
778 https://doi.org/10.1002/rse2.325, 2023.
779 Rai, P. and Singh, J. S.: Invasive alien plant species: Their impact on environment, ecosystem
780 services and human health, Ecol. Indic., 2020, 20 pages,
781 https://doi.org/10.1016/j.ecolind.2019.106020, 2020.
782 Rakotoarivony, M. N. A., Gholizadeh, H., Hammond, W. M., Hassani, K., Joshi, O., Hamilton,
783 R. G., Fuhlendorf, S. D., Trowbridge, A. M., and Adams, H. D.: Detecting the invasive
784 Lespedeza cuneata in grasslands using commercial small satellite imagery, Int. J. Remote
785 Sens., 44, 6802–6824, https://doi.org/10.1080/01431161.2023.2275321, 2023.
786 Van Rees, C. B., Hand, B. K., Carter, S. C., Bargeron, C., Cline, T. J., Daniel, W., Ferrante, J.
787 A., Gaddis, K., Hunter, M. E., Jarnevich, C. S., McGeoch, M. A., Morisette, J. T., Neilson,
788 M. E., Roy, H. E., Rozance, M. A., Sepulveda, A., Wallace, R. D., Whited, D., Wilcox, T.,
789 Kimball, J. S., and Luikart, G.: A framework to integrate innovations in invasion science for
790 proactive management, Biol. Rev., 97, 1712–1735, https://doi.org/10.1111/brv.12859, 2022.
791 Riggs, G. A., Hall, D. K., Román, M. O., and others: MODIS snow products collection 6 user
792 guide, Natl. Snow Ice Data Cent. Boulder, CO, USA, 66, 2015.
793 Saraf, S., John, R., Goljani Amirkhiz, R., Kolluru, V., Jain, K., Rigge, M., Giannico, V., Boyte,
794 S., Chen, J., Henebry, G., Jarchow, M., and Lafortezza, R.: Biophysical drivers for predicting
795 the distribution and abundance of invasive yellow sweetclover in the Northern Great Plains,
796 Landsc. Ecol., 38, 1463–1479, https://doi.org/10.1007/s10980-023-01613-1, 2023.
797 Saraf, S., John, R., Kolluru, V., Jain, K., Henebry, G., Chen, J., and Lafortezza, R.:
798 Spatiotemporal mapping of invasive yellow sweetclover blooms using Sentinel-2 and high-
799 resolution drone imagery, https://doi.org/10.6084/m9.figshare.29270759, 2025.
800 Spiess, J., McGranahan, D., Geaumont, B., Sedivec, K., Lakey, M., Berti, M., Hovick, T., and
801 Limb, R.: Patch-Burning Buffers Forage Resources and Livestock Performance to Mitigate
802 Drought in the Northern Great Plains, Rangel. Ecol. Manag., 73,
803 https://doi.org/10.1016/j.rama.2020.03.003, 2020.
804 Stohlgren, T. J., Ma, P., Kumar, S., Rocca, M., Morisette, J. T., Jarnevich, C. S., and Benson, N.:
805 Ensemble habitat mapping of invasive plant species, Risk Anal., 30, 224–235,

https://doi.org/10.5194/essd-2025-353
Preprint. Discussion started: 4 August 2025

https://doi.org/10.1111/j.1539-6924.2009.01343.x, 2010.
Strashok, O., Ziemiańska, M., and Strashok, V.: Evaluation and Correlation of Sentinel-2 NDVI and NDMI in Kyiv (2017-2021), J. Ecol. Eng., 23, 212–218, https://doi.org/10.12911/22998993/151884, 2022.
Sulik, J. J. and Long, D. S.: Spectral considerations for modeling yield of canola, Remote Sens. Environ., 184, 161–174, https://doi.org/https://doi.org/10.1016/j.rse.2016.06.016, 2016.
Thornton, M. M., Shrestha, R., Wei, Y., Thornton, P. E., and Kao, S.-C.: Daymet: Monthly Climate Summaries on a 1-km Grid for North America, Version 4 R1, https://doi.org/10.3334/ORNLDAAC/2131, 2022.
Trimble Inc. (n.d.): Trimble DA2 GNSS Receiver, https://geospatial.trimble.com/en/products/hardware/trimble-da2, 2025.
Turner, D. and Wallace, L.: Direct Georeferencing of Ultrahigh-Resolution UAV Imagery, IEEE Trans. Geosci. Remote Sens., 52, https://doi.org/10.1109/TGRS.2013.2265295, 2013.
Varner, C.: Invasive Flora of the West Coast: British Columbia and the Pacific Northwest, Heritage House Publishing Co., University of Washington Press, 2022.
Vidiella, P. E., Armesto, J. J., and Gutiérrez, J. R.: Vegetation changes and sequential flowering after rain in the southern Atacama Desert, J. Arid Environ., 43, 449–458, https://doi.org/https://doi.org/10.1006/jare.1999.0565, 1999.
Winkler, D. E. and Brooks, E.: Tracing Extremes across Iconic Desert Landscapes: Socio-Ecological and Cultural Responses to Climate Change, Water Scarcity, and Wildflower Superblooms, Hum. Ecol., 48, 211–223, https://doi.org/10.1007/s10745-020-00145-5, 2020.
Wolf, J. J., Beatty, S. W., and Carey, G.: Invasion by Sweet Clover (Melilotus) in Montane Grasslands, Rocky Mountain National Park, Ann. Assoc. Am. Geogr., 93, 531–543, https://doi.org/10.1111/1467-8306.9303001, 2003.
Wolter, K. M.: The Jackknife Method BT - Introduction to Variance Estimation, edited by: Wolter, K. M., Springer New York, New York, NY, 151–193, https://doi.org/10.1007/978-0-387-35099-8_4, 2007.
Wurtz, T. L., Macander, M. J., and Spellman, B. T.: Spread of Invasive Plants From Roads to River Systems in Alaska: A Network Model, U S For. Serv. Pacific Northwest Res. Stn. Gen. Tech. Rep. PNW-GTR, 699–708, 2010.
Zar, J. H.: Spearman rank correlation, Encycl. Biostat. Wiley Online Libr., 7, 2005.
Zhang, Z., Bao, T., Hautier, Y., Yang, J., Liu, Z., and Qing, H.: Microclimate complexity in temperate grasslands: implications for conservation and management under climate change, Ecol. Evol., 12, e9385, https://doi.org/https://doi.org/10.1002/ece3.9385, 2022.

https://doi.org/10.5194/essd-2025-353
Preprint. Discussion started: 4 August 2025

841 **Tables and Figures**

842

843 Table 1. Details of the drone flights covered in sample collection for summer 2023.

Site	Date	Spatial Resolution (m)	Area (ha)	Sampling
1	July 9	0.06	10.5	Validation
2	July 9	0.03	1.9	Training
3	July 10	0.04	4.9	Training
4	July 10	0.04	4.1	Training
5	July 11	0.07	30.5	Training
6	July 11	0.04	3.2	Training
7	July 12	0.05	7.2	Training
8	July 12	0.03	3	Training
9	July 13	0.04	4.9	Validation
10	July 13	0.04	4.6	Validation
11	July 14	0.03	4.2	Training
12	July 14	0.05	7.2	Training
13	July 15	0.05	10.5	Training
14	July 15	0.04	4.7	Validation

844

https://doi.org/10.5194/essd-2025-353
Preprint. Discussion started: 4 August 2025

845 Table 2. Description of 13 independent variables selected for estimating the yellow sweetclover
846 cover (%)

S.No	Independent Variables	Codes	Resolution
1	Mean annual precipitation	MAP	1 km
2	Mean annual precipitation (coefficient of variation)	MAPcv	1 km
3	Mean annual temperature	MAT	1 km
4	Mean annual precipitation (coefficient of variation)	MATcv	1 km
5	Snow Depth	SnowDepth	500m
6	Snow Depth (coefficient of variation)	SnowDepth_cv	500m
7	Elevation	Elevation	10m
8	Slope	Slope	10m
9	Proximity to roads	Dist_Roads	30m
10	Normalized Difference Moisture Index	NDMI	10m
11	Normalized Difference Water Index (coefficient of variation)	NDWIcv	10m
12	Land Surface Water Index (coefficient of variation)	LSWIcv	10m
13	Tasseled Cap Wetness (coefficient of variation)	TCWcv	10m

847

https://doi.org/10.5194/essd-2025-353
Preprint. Discussion started: 4 August 2025

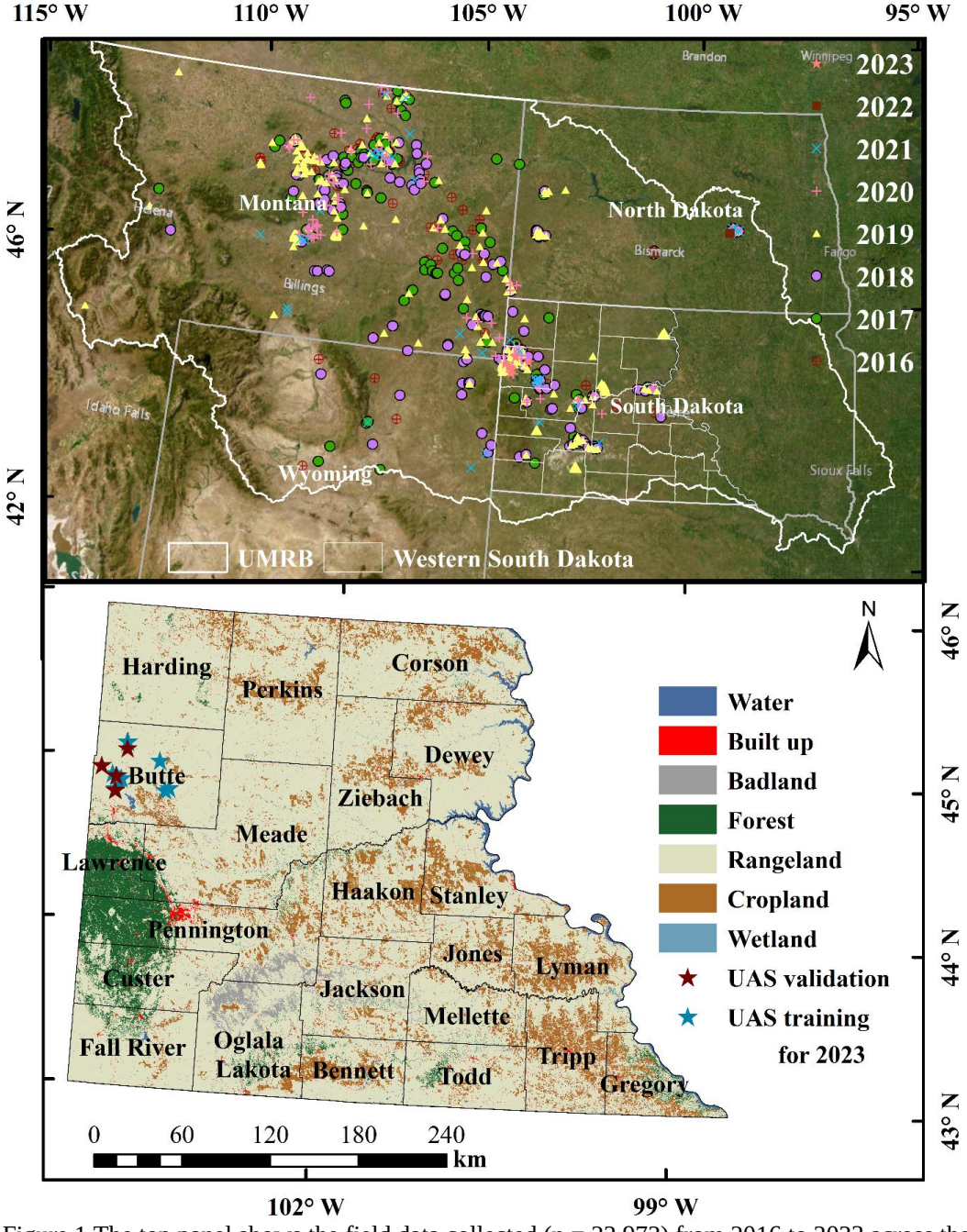

Figure 1 The top panel shows the field data collected (n = 22,972) from 2016 to 2023 across the Northern Great Plains (© Esri, Maxar, Earthstar Geographics, and the GIS User Community). The second panel shows the UAS training and validation sites overlaid on land cover map with county boundaries of western South Dakota.

https://doi.org/10.5194/essd-2025-353
Preprint. Discussion started: 4 August 2025

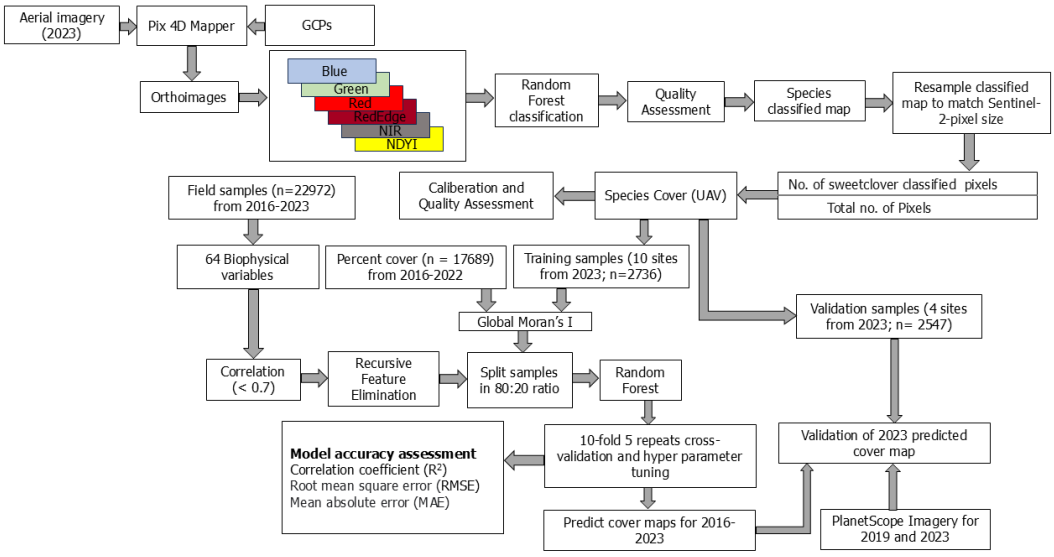

Figure 2 Workflow to predict invasive yellow sweetclover percent cover at 10m resolution using UAS and ancillary data for 2016-2023.

https://doi.org/10.5194/essd-2025-353
Preprint. Discussion started: 4 August 2025

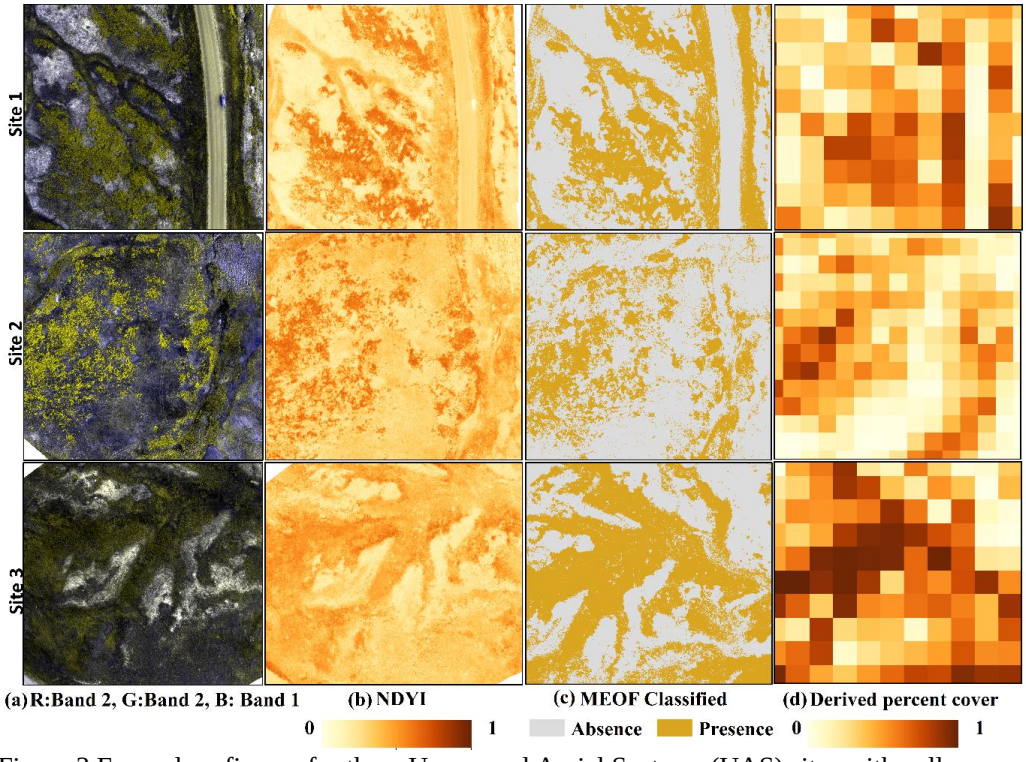

Figure 3 Exemplary figures for three Unmanned Aerial Systems (UAS) sites with yellow sweetclover (MEOF) blooms (a) UAS orthoimages in green, green and blue band combination (b) Normalized Difference Yellowness Index (c) Random Forest classified image showing yellow sweetclover presence and absence (d) yellow sweetclover cover derived at 10m pixel size.

https://doi.org/10.5194/essd-2025-353
Preprint. Discussion started: 4 August 2025

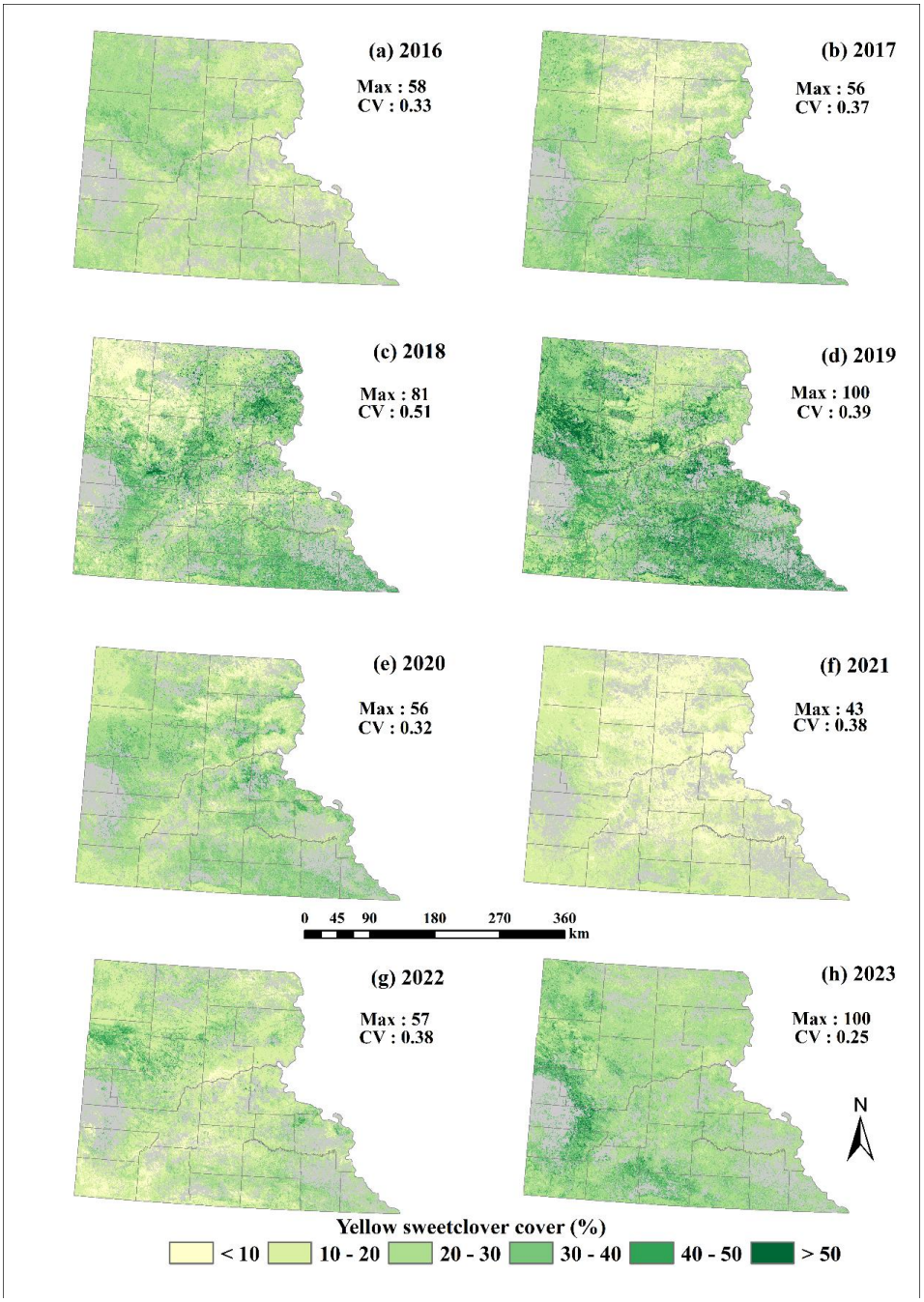

Figure 4 Predicted yellow sweetclover maps using a generalized Random Forest regression model for 2016-2023.

https://doi.org/10.5194/essd-2025-353
Preprint. Discussion started: 4 August 2025

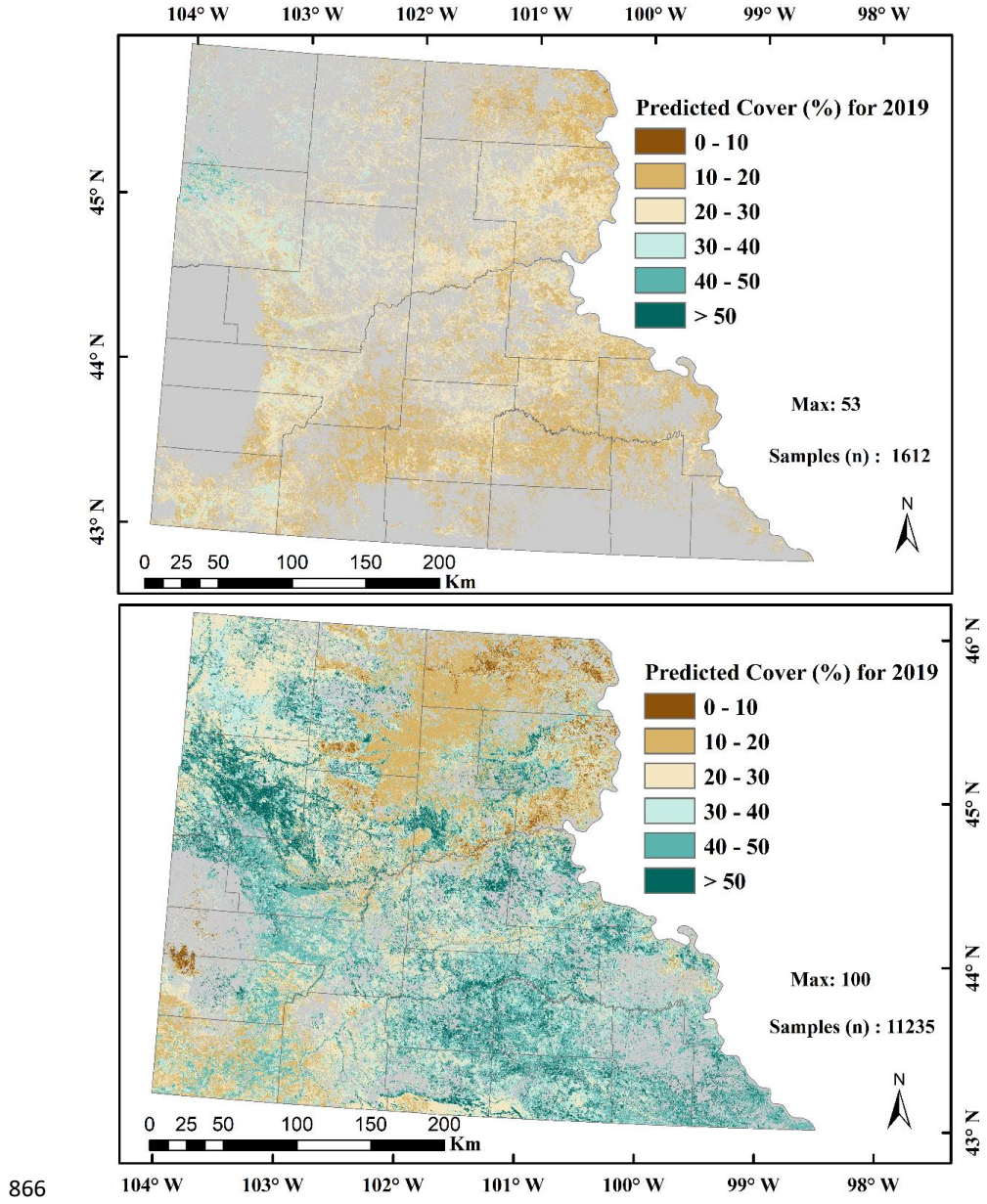

Figure 5 (a) Yellow sweetclover percent cover estimates in the high yellow sweetclover probability of occurrence regions in the western South Dakota rangelands for 2019 using 1,612 samples (Saraf et al., 2023), (b) Yellow sweet clover predicted for 2019 using 11,235 samples in the western South Dakota rangelands.

https://doi.org/10.5194/essd-2025-353
Preprint. Discussion started: 4 August 2025

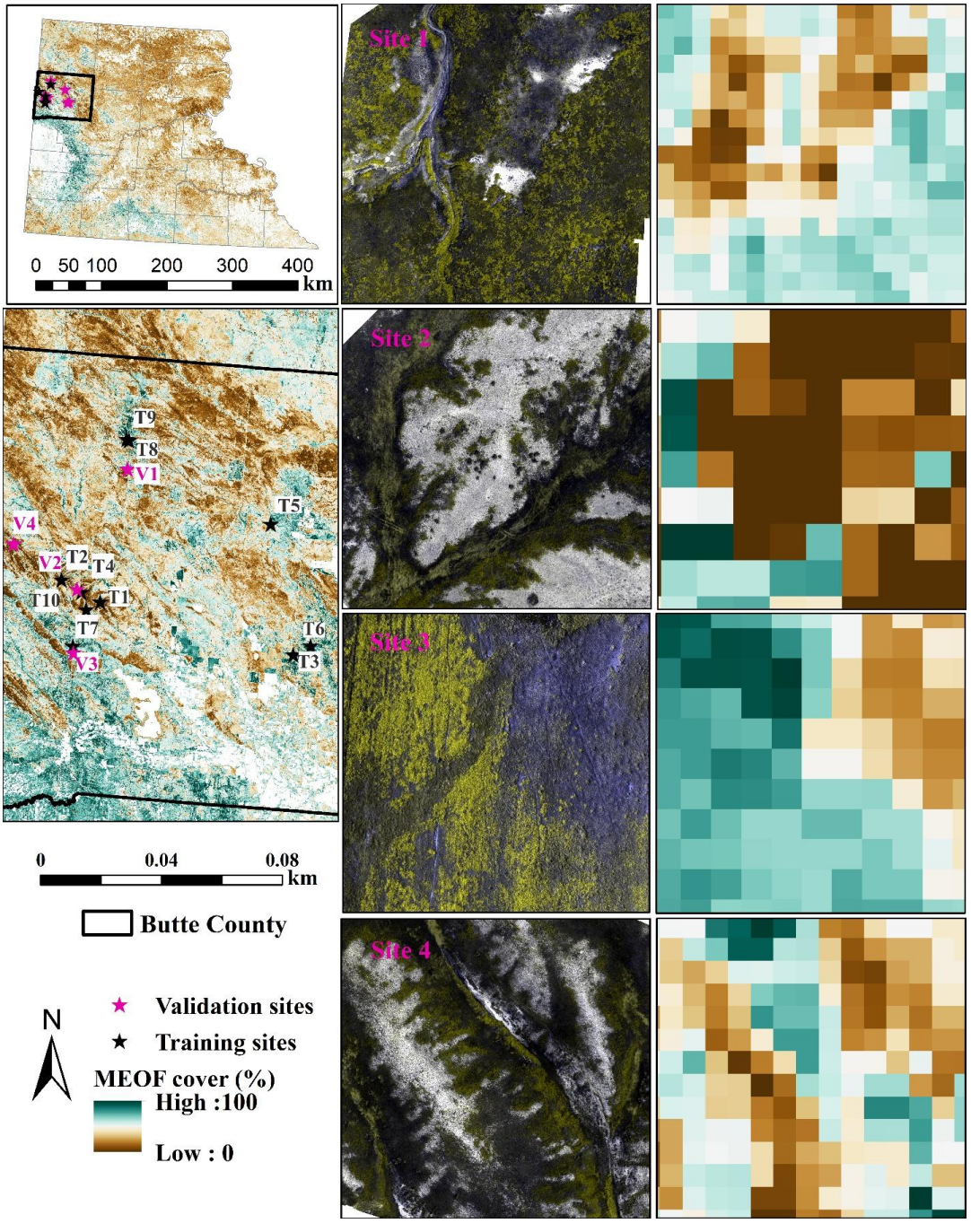

871

872 Figure 6. Percent cover estimates for invasive yellow sweetclover for four independent UAS
873 validation sites shown in green-green-blue false color combination to highlight yellow
874 sweetclover blooms.

https://doi.org/10.5194/essd-2025-353
Preprint. Discussion started: 4 August 2025

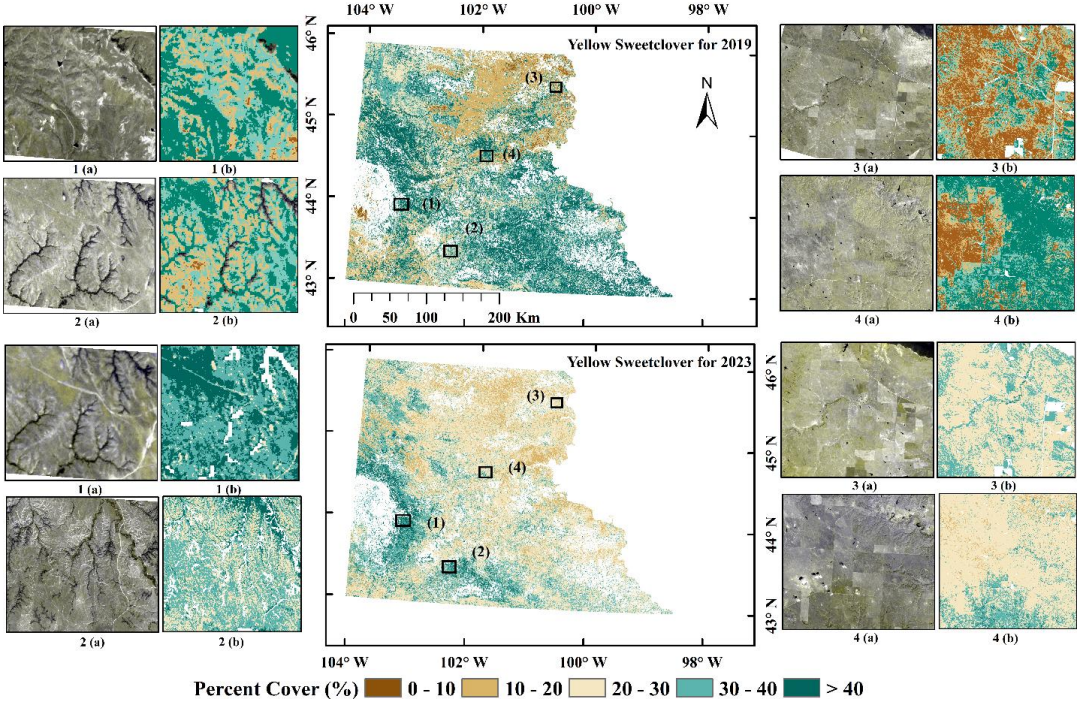

Figure 7. Predicted percent cover estimates for invasive yellow sweetclover (MEOF) in panel (a) at four different sites represented with numbers and each site is compared with the PlanetScope imagery available at 3 m resolution shown in green, green, and blue band combination to highlight yellow sweetclover blooms in panel (b). (PlanetScope imagery © Planet Labs PBC).